ELSEVIER

Palaeogeography, Palaeoclimatology, Palaeoecology 201 (2003) 283–306

PALAEO

www.elsevier.com/locate/palaeo

Milankovitch climatic signals in Lower Triassic (Olenekian) peritidal carbonate successions, Nanpanjiang Basin, South China

Wan Yang [a,*], Daniel J. Lehrmann [b]

[a] *Department of Geology, Wichita State University, Wichita, KS 67260, USA*
[b] *Department of Geology, University of Wisconsin, Oshkosh, WI 54901, USA*

Received 5 March 2002; received in revised form 9 July 2003; accepted 14 August 2003

Abstract

Meter-scale peritidal carbonate strata from an isolated platform in the Nanpanjiang Basin of South China were tested for the presence of periodic or quasi-periodic climatic signals. These signals provide information on factors controlling cyclic sedimentation in the equatorial eastern Tethys during the Early Triassic greenhouse period. Parasequences are composed of shallowing-upward successions of subtidal facies, including skeletal packstone and grainstone, calcimicrobial boundstone, and oolitic packstone and grainstone, intertidal laminated lutite and ribbon rock, and rare supratidal microbial laminite. Parasequence stacking patterns display three orders of cyclicity, suggesting hierarchical stratigraphic relationships. Gamma analysis of Kominz and Bond [Earth Planet. Sci. Lett. 48 (1990) 233–244] was used to estimate facies-dependent thickness–time conversion factors (i.e. γs), and to construct γ-tuned and γ-untuned time series for two stratigraphic sections. Spectra of these time series indicate the presence of quasi-periodic signals, with prominent short-eccentricity (94.9–131.2 kyr), short-obliquity (35.8 kyr), and long-precessional index (21.2 kyr) peaks, and minor long-eccentricity (412.9 kyr), long-obliquity (45.3 kyr), short-precessional index (17.7 kyr), and constructional-tone (9.7 kyr) peaks when calibrated on the γ-tuned spectra. Thus, Milankovitch climatic forcing probably greatly influenced sedimentation. The calibration indicates that the subtidal facies has a sedimentation rate of 24.6–30.7 cm/kyr and the intertidal–supratidal facies has a rate of 2.7–6.0 cm/kyr. The estimated duration of deposition of the two sections is 1139–1423 kyr, and corresponds to a stratigraphic completeness of 32–92%. The completeness is much greater than that of icehouse stratigraphic records. We speculate that variations in carbonate productivity and environmental conditions driven by Milankovitch climatic forcing, combined with low-amplitude sea-level fluctuations, were likely major controls on cyclic sedimentation. Furthermore, evolutional spectra of the two sections show that dominant Milankovitch climatic forcings varied from short-eccentricity, obliquity, to long-precessional index during the course of sedimentation. Some spectral differences between the two sections suggest variations in depositional/recording mechanisms of Milankovitch climatic signals between platform interior and windward platform margin.
© 2003 Elsevier B.V. All rights reserved.

Keywords: Peritidal carbonate; Early Triassic; China; Milankovitch; spectral analysis

* Corresponding author. Tel.: +1-316-978-7241; Fax: +1-316-978-7229.
E-mail address: wan.yang@wichita.edu (W. Yang).

0031-0182/03/$ – see front matter © 2003 Elsevier B.V. All rights reserved.
doi:10.1016/S0031-0182(03)00614-X

1. Introduction

The Early Triassic was a period of greenhouse climate (Berner, 1991; Frakes et al., 1992) on the supercontinent Pangea and the superanoxic ocean Panthalassa (Isozaki, 1994, 1997). Milankovitch signals have been detected quantitatively in Late Triassic lacustrine records of North America (e.g. Olsen, 1986; Kominz and Bond, 1990; Kent and Olsen, 2000), and in Middle and Late Triassic peritidal carbonate records (e.g. Fischer, 1964; Goldhammer et al., 1990; Hinnov and Goldhammer, 1991; Preto et al., 2001). In addition, several qualitative studies have suggested Milankovitch climatic forcing on cyclic sedimentation in marine settings during the Early Triassic (e.g. Broglio Loriga et al., 1986, 1990; Bottjer and Schubert, 1997; Yu et al., 1998; Twitchett, 1999; Woods et al., 1999). However, quantitative tests of Milankovitch climatic signals in Early Triassic marine records are lacking. Whether Milankovitch orbital forcing was a major climatic driver during this time is essential to understanding the controlling factors and depositional mechanisms of peritidal cyclic carbonate sedimentation, and the shallow marine environments associated with the prolonged biotic recovery after the end-Permian mass extinction (Flügel, 1982; Flügel and Stanley, 1984; Stanley, 1988; Schubert and Bottjer, 1992; Wignall and Hallam, 1992, 1996; Knoll et al., 1996; Twitchett and Wignall, 1996; Bottjer and Schubert, 1997; Twitchett, 1999; Woods et al., 1999).

In this study, two Lower Triassic cyclic peritidal carbonate sections on an isolated carbonate platform, the Great Bank of Guizhou (GBG), in the Nanpanjiang Basin of South China were analyzed to test whether Milankovitch signals are present in a pure carbonate system in a greenhouse climate (Fig. 1; Lehrmann et al., 1998, 2001). The sections consist of meter-scale shallowing-upward parasequences containing subtidal *Renalcis* reef mounds, skeletal or oolitic packstone capped by intertidal, flaser-bedded ribbon rock. They are substantially different from other Lower Triassic successions that consist of lithologically monotonous, low-biodiversity, skeletal wackestones, packstones or oolitic grainstones and thinly bedded lime mudstones, with interbedded siliciclastics (cf. Broglio Loriga et al., 1986; Schubert and Bottjer, 1995). They are also different from other Lower Triassic cyclic sections that lack *Renalcis* reef mounds (Wignall and Hallam, 1992; cf. Lehrmann et al., 2001). A spectral analysis of these sections is particularly useful for evaluating Milankovitch forcing on climatic and oceanic conditions in a mid-ocean position in the equatorial eastern Tethys (e.g. Kutzbach et al., 1990; Crowley et al., 1992; Parrish, 1993; Kutzbach, 1994).

Several authors have suggested that perturbations in shallow-marine oceanic conditions (e.g. deleterious anoxia, or high CO_2 concentrations) may have contributed to the end-Permian extinction and prolonged biotic recovery until the end of the Early Triassic (cf. Isozaki, 1994; 1997; Knoll et al., 1996; Woods et al., 1999; Lehrmann et al., 2001). This study will provide constraints on the unusual environmental and oceanic conditions in the aftermath of the end-Permian mass extinction.

2. Geology

2.1. Tectonic and depositional setting

The Lower Triassic peritidal cyclic limestone occurs in the interior of the isolated GBG in the Nanpanjiang Basin, South China (Fig. 1; Lehrmann et al., 1998, 2001). The Nanpanjiang Basin is bordered on the north and west by the vast carbonate Yangtze Platform, and faced the Tethys to the east and south. The entire region resides on the Yangtze Plate (Enos, 1995; Xü et al., 1997), which was located in the eastern Tethys near the equator during the Early Triassic and experienced progressive rotation, northward migration, and eventual docking with the North China Plate from the Late Permian to Late Triassic or Early Jurassic (Klimetz, 1983; Sengör, 1987; Enkin et al., 1992; Enos, 1995; Li, 1998; Sun et al., 1989).

The GBG evolved from a low-relief bank with 50–100 m relief, rimmed with oolite shoals and gentle basin–margin slopes in the Early Triassic

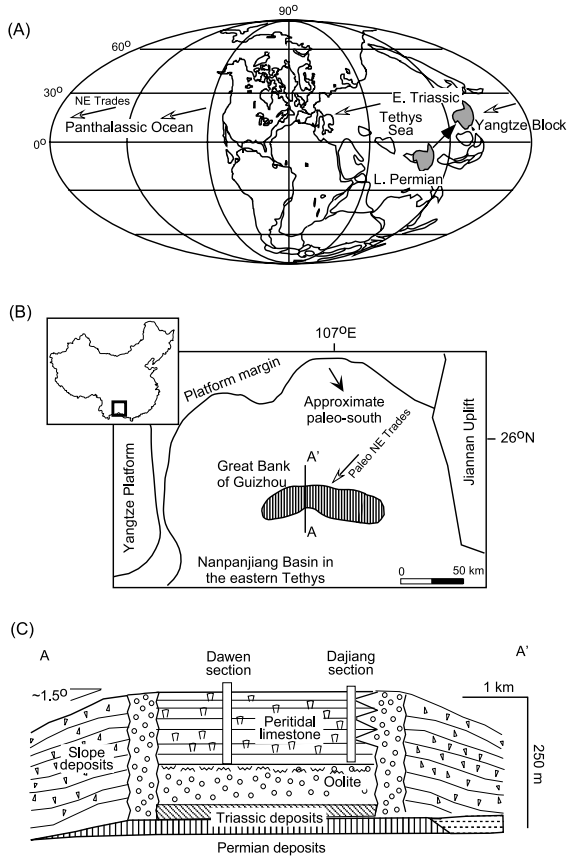

Fig. 1. (A) Paleogeographic location of the Yangtze Block at about 12°N latitude, which had migrated across the paleoequator from the end of the Permian to the Early Triassic. Modified from Scotese (1994). (B) Early Triassic paleogeographic map of the Nanpanjiang Basin compiled from regional geologic maps of Guizhou Bureau (1987) and Guangxi Bureau (1985), showing location of the GBG. (C) Restored cross-section of Lower Triassic strata in the GBG, showing stratigraphic architecture and location of the Dawen and Dajiang sections. The cross-section location is shown in panel B. Modified from Lehrmann et al. (2001).

(Fig. 1C), to a *Tubiphytes* reef-rimmed platform with more than 400-m relief and steep basin–margin slopes in the Middle Triassic (Anisian–early Ladinian) and, finally, to a high-relief erosional escarpment before the platform was drowned and buried with siliciclastic turbidites at the beginning of the Late Triassic (Lehrmann et al., 1998).

The Lower Triassic architecture of the GBG is a low-relief isolated carbonate bank with gently sloping basin–margin strata (Fig. 1C). The strata in the shallow-water facies of the flat-topped platform interior are 265 m thick, composed of subtidal to peritidal lime mudstone, dolo-oolite grainstone, overlain by peritidal cyclic limestone. The platform–margin shoals are composed of oolitic packstone and grainstone. The basin–slope strata are composed of pelagic lime mudstone, debris-flow carbonate breccia, and turbidite grainstone and packstone (Lehrmann et al., 1998, 2001). The age of the peritidal cyclic limestone is constrained to the Olenekian by the occurrence of the conodont *Lonchodina nevadensis* on the platform and *Neospathodus timorensis*, an index fossil for the Scythian–Anisian boundary, at the platform margin (Lehrmann, 1993). Lehrmann et al. (2001) found that the Lower Triassic platform interior succession contains fabrics consistent with shallow subtidal to peritidal conditions and interpreted that the Olenekian cyclic limestone facies were deposited in relatively low-energy, restricted- to normal-marine, shallow subtidal and peritidal environments.

2.2. Lithofacies and depositional environments

This study focuses on Olenekian peritidal cyclic limestone in the Dawen and Dajiang sections on the GBG (Figs. 1C and 2). The Dawen section is 164 m thick and contains 83 parasequences ranging from 0.2 to 7.1 m thick. The Dajiang section is 137 m thick and contains 64 parasequences ranging from 0.25 to 7.4 m thick. An 'ideal parasequence' has a skeletal packstone or oolite base overlain by calcimicrobial mounds, and capped by flaser-bedded ribbon rock (Fig. 2C). Variations from the ideal parasequence include those with calcimicrobial facies at the base, those lacking calcimicrobial mounds, or those capped by a microbial laminite rather than ribbon rock. The detailed facies description and interpretation by Lehrmann et al. (2001) are summarized below:

Skeletal packstone is the most abundant facies (Figs. 2 and 3). It is dark gray to tan and typically massive. Skeletal grains include thin-shelled bivalves, gastropods, ostracodes, foraminifera, minor echinoderm fragments, and sparse lingulid brachiopods and spirorbid worm tubes. This fa-

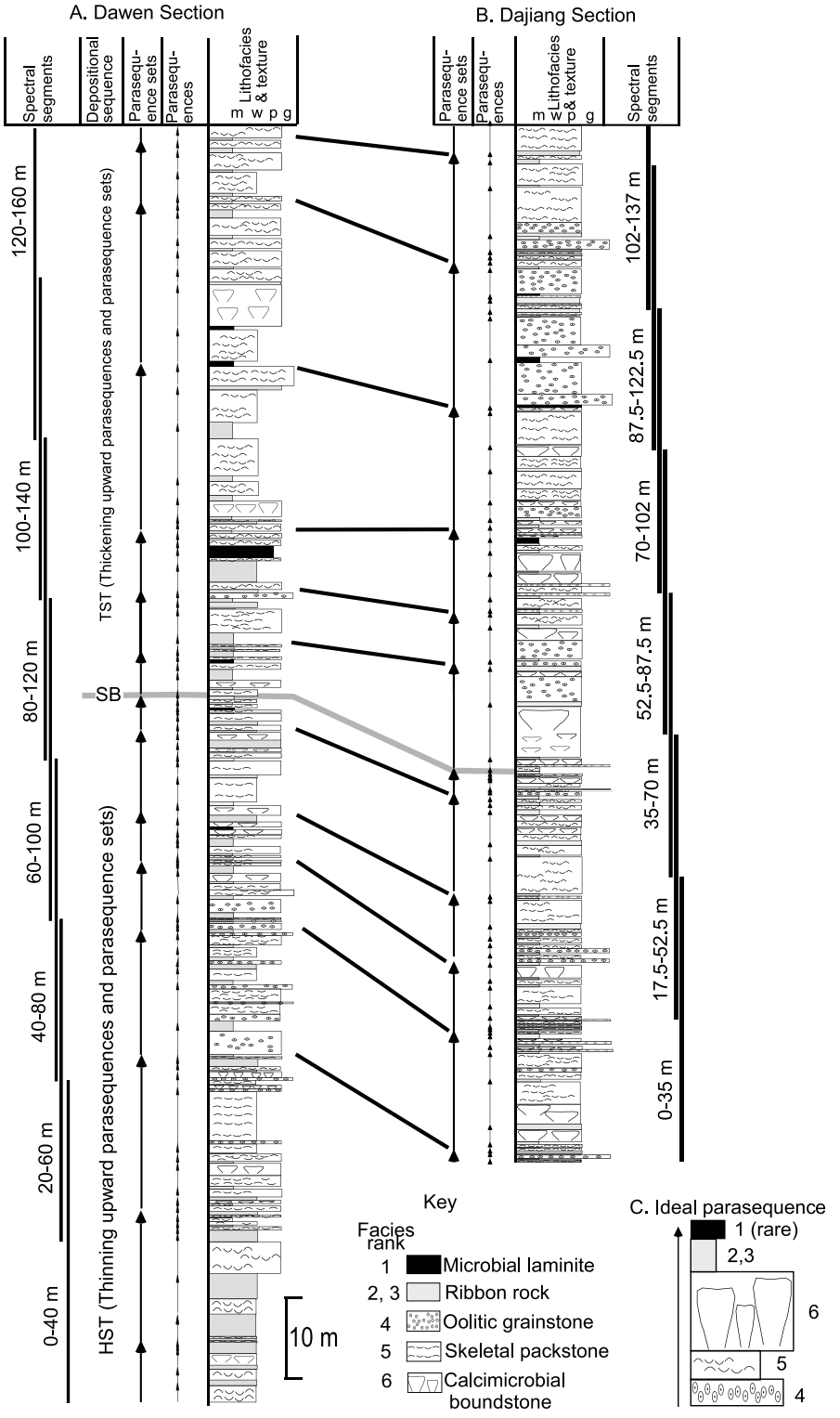
A. Dawen Section
B. Dajiang Section
Spectral segments
Depositional sequence
Parasequence sets
Parasequences
Lithofacies & texture
m w p g
120-160 m
100-140 m
80-120 m
60-100 m
40-80 m
20-60 m
0-40 m
TST (Thickening upward parasequences and parasequence sets)
SB
HST (Thinning upward parasequences and parasequence sets)
102-137 m
87.5-122.5 m
70-102 m
52.5-87.5 m
35-70 m
17.5-52.5 m
0-35 m
10 m
Key
Facies rank
1 Microbial laminite
2, 3 Ribbon rock
4 Oolitic grainstone
5 Skeletal packstone
6 Calcimicrobial boundstone
C. Ideal parasequence
1 (rare)
2,3
6
5
4

cies is interpreted to represent open to restricted shallow-subtidal environments with relatively low current energy. The presence of echinoderms suggests occasional open-marine circulation. The abundance of lime mud indicates low-energy conditions.

Oolitic packstone and grainstone are more common in the Dajiang section located at the windward edge of the platform than in the Dawen section in the platform interior (Figs. 2 and 3). It is light gray or tan and thin to medium bedded. Most of the oolite is packstone. Peloids, bivalve fragments, and imbricated flat-pebble conglomerates are locally abundant. Grainstone fabrics and imbricated intraclasts indicate a current-swept shoal environment. Common infiltrated mud fabrics suggest shoal stabilization and shift to lower-energy conditions in the upper parts of oolite beds.

Biostromes and bioherms composed of calcimicrobial boundstone occur in the middle and base of parasequences immediately below parasequence cap facies (Figs. 2 and 3). The boundstone is dark gray with light-gray splotches, composed of a dark-colored framework surrounding light-gray to tan internal cavities. The framework is composed of globular micritic fossils with a morphology similar to the calcified cyanobacteria *Renalcis* (Lehrmann, 1999; Lehrmann et al., 2001). The calcimicrobial boundstone was interpreted to have formed as organic mound and bioherm constructions in open to restricted marine environments characterized by low biodiversity (Lehrmann, 1999).

Flaser-bedded and horizontally burrowed ribbon rock is the most common cap facies (Figs. 2 and 3). It is dark gray to tan and consists of laminated and flaser-bedded interlayers of lime mudstone and peloid-skeletal grainstone. Horizontal burrows occur locally with minimal disruption of surrounding laminae. Scoured surfaces are commonly overlain by imbricated intraclasts and convolute lamination formed by soft sediment deformation. Opposed current indicators suggest reversing currents. Discontinuous lime mudstone layers and drapes over ripple forms and grainstone lenses are ubiquitous. The ribbon rocks represent muddy tidal flats dominated by intertidal conditions. Scours and ripples formed during tide advance or retreat; lime mud drapes formed during slack tide. The rarity of desiccation features suggests predominantly intertidal rather than supratidal conditions.

Microbial laminite occurs sparsely in parasequence caps in the upper parts of the Dawen and Dajiang sections only (Figs. 2 and 3). The laminite contains wrinkly microbial laminite layers and shows evidence of desiccation, such as water escape structures and prism cracks and autoclastic breccia layers with reddened clasts, calcareous soil concretions, and minor irregular fenestrae. This facies represents supratidal conditions and prolonged exposure of the tidal flats, which were rare during the deposition of the Dawen and Dajiang cycles.

2.3. Hierarchical parasequence stacking patterns

Stacking of individual shallowing-upward parasequences represents repeated upward shallowing from shallow subtidal, open to restricted-marine conditions to predominantly intertidal conditions on muddy tidal flats and rarely to supratidal conditions. A larger-scale pattern is manifested by systematic variations in parasequence thickness. Parasequences progressively thin upward in the lower parts of both sections and a cluster of thin parasequences underlie a sequence boundary (SB) in the middle parts of the sections (Fig. 2A,B). The parasequences then progressively

Fig. 2. Lithostratigraphic columns of Lower Triassic strata in (A) Dawen and (B) Dajiang sections. Three orders of cycles, namely parasequences, parasequence sets, and depositional sequences, were identified. Systems tracts and SB of depositional sequences are indicated. TST, transgressive systems tract; HST, highstand systems tract; SB, sequence boundary. Vertical bars indicate segments of evolutional spectra. Dashed line indicates tentative correlation. The typical or 'ideal' parasequence is shown in panel C. Modified from Lehrmann et al. (2001). Facies ranks are interpreted relative water depth of component lithofacies from Lehrmann et al. (2001).

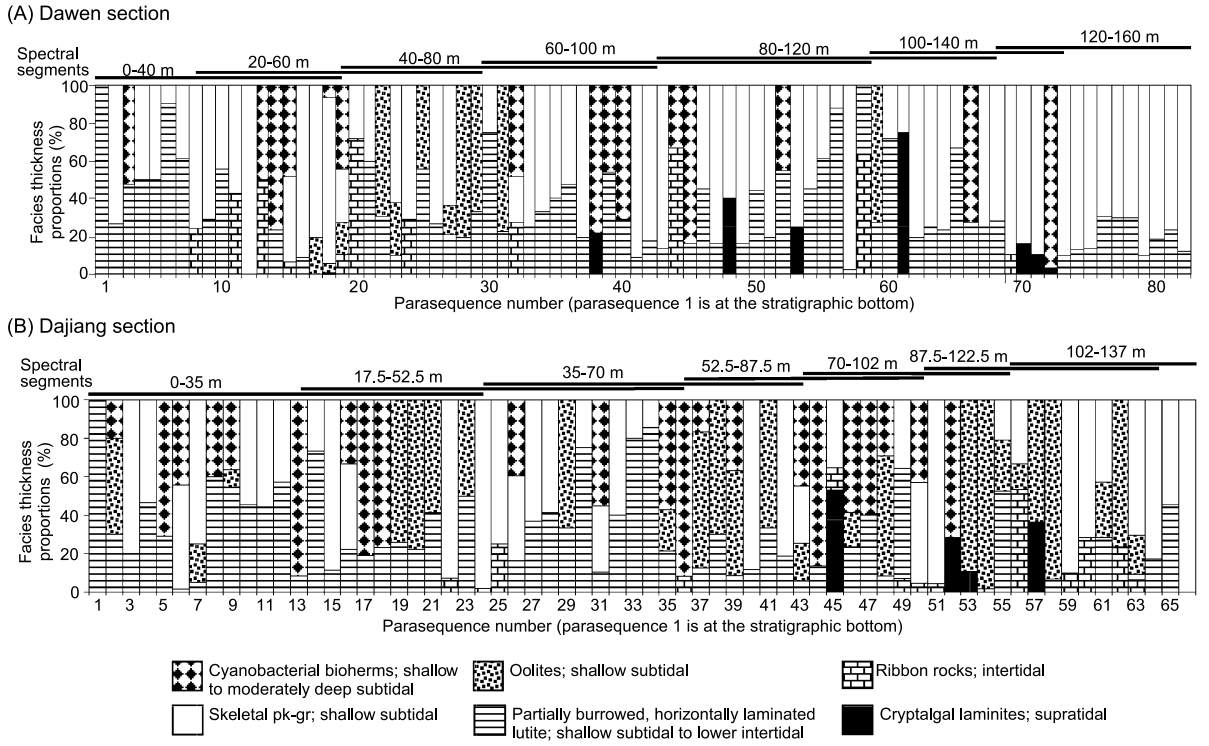

Fig. 3. Facies composition of Dawen (A) and Dajiang (B) parasequences. Dajiang parasequences have more diverse facies composition than Dawen parasequences, because the Dajiang section is located close to the windward platform edge and, thus, had been subject to more dynamic wave and wind actions and storm-induced oolite spill-over lobes than the Dawen section located in the platform interior.

thicken upward from the SB. The thinning-then-thickening pattern may either represent a long-term change in accommodation space or in subtidal carbonate productivity (Yang and Lehrmann, 2001; Yang et al., 2002; cf. Goldhammer et al., 1990; Lehrmann and Goldhammer, 1999; Lehrmann et al., 2001).

Two estimates of the duration of the Olenekian Stage (2.125 and 3 Myr) were derived from recently published age dates. Recent zircon U–Pb age dates that have resulted in major changes in the Triassic time scale include: (1) a Permian–Triassic boundary age of 251.3–253 Ma (Bowring et al., 1998; Mundil et al., 2001); (2) an Olenekian–Anisian boundary of 247 Ma (Martin et al., 2001); and (3) an Anisian–Ladinian boundary age of 240.5–241 Ma (Mundil et al., 1996; Palfy et al., 2002). The analytical accuracy of these ages ranges from ±0.3 to 0.6 Myr. The duration of the Early Triassic (Scythian) is thus estimated to be 4.3–6 Myr (253–247 Ma or 251.3–247 Ma). Considering the analytical uncertainties, the duration may range from 3.1 to 7.2 Myr (i.e. an overestimate or underestimate of 1.2 Myr resulting from an analytical error of ±0.6 Myr at the lower and upper boundaries). The Induan–Olenekian boundary has not yet been dated; we thus interpolate the boundary at the midpoint of the Early Triassic on the basis of equal number of ammonoid zones in the two stages of the Early Triassic (cf. techniques employed in Harland et al., 1989). With these assumptions, the mean duration of the Olenekian is thus estimated to be 2.125 or 3 Myr. Considering the analytical error limits, the range of duration of the Olenekian is from 1.55 to 3.6 Myr.

The estimated duration of the Dawen and Dajiang successions (Olenekian) at 2.125 or 3 Myr

thus places the large-scale cycles (termed depositional sequences in this study) in the third order (1–10 Myr) and the small-scale primary cycles (termed parasequences in this study) in the fifth order (0.01–0.1 Myr) (Lehrmann et al., 2001).

The repeated clustering of thin and thick parasequences defines 14 parasequence sets in fourth order (0.1–1 Myr), suggesting thickness bundling of parasequences into parasequence sets (Fig. 2). The number of parasequences in a parasequence set changes systematically from a maximum of eight in the highstand systems tract (HST) and transgressive systems tract (TST) to a minimum of three near the SB. Yu et al. (1998) postulated that the bundling suggests Milankovitch forcing during parasequence formation. Parasequence sets also change systematically in thickness from a maximum of 18 m in the HST and TST to a minimum of 4.3 m in the minimum accommodation zone near the SB (Fig. 2; Lehrmann et al., 2001). The hierarchical stacking of parasequences, parasequence sets, and depositional sequences suggests allogenic controlling processes acting at variable time scales during cyclic sedimentation of the Dawen and Dajiang sections (cf. Barrell, 1917; Goldhammer et al., 1990, 1993; Read, 1995; Kerans and Tinker, 1997, among many others).

Lehrmann and Goldhammer (1999) performed Markov chain analysis, run tests, and Durbin–Watson analysis on parasequence stacking patterns in stratigraphic sections, all of which indicated statistical order and non-randomness in the vertical facies successions and parasequence thickness. The hierarchical stacking patterns and the speculations of Milankovitch climatic forcing of previous studies (e.g. Yu et al., 1998) prompted the spectral analysis in this study to search for periodic or quasi-periodic signals in the Dawen and Dajiang sections and to test the possibility of a Milankovitch climatic origin of the cyclicity.

3. Testing the periodicity of the Dawen and Dajiang sections

Spectra of the Dawen and Dajiang sections were estimated in order to compare the periods and relative amplitudes of the spectral peaks with those of major Early Triassic Milankovitch cycles. A section is represented by a facies curve with facies types ranked by interpreted environment as the horizontal axis and thickness as the vertical axis (Fig. 4). Spectral analysis was carried out in three steps: (1) the facies curve in thickness was converted into a time series using gamma analysis (explained below); (2) the spectra of the time series were calculated, including evolutional spectra of segments of each section; and (3) the spectral peaks were calibrated to obtain their periods, which were then compared with those of the Milankovitch climatic cycles.

3.1. Thickness–time conversion using gamma analysis

Thickness–time conversion can be done by assuming a constant sedimentation rate for the entire section. The spectrum of the resulting time series may, or may not, show indications of Milankovitch signals, because component lithofacies have different sedimentation rates. The true time series of a section is different from the spatial series and, thus, the spectrum of the time series will differ from that of the spatial series (e.g. Yang and Kominz, 1999). Exact sedimentation rates of individual facies are difficult to obtain. Serious efforts, however, have been made to achieve more accurate thickness–time conversions (e.g. Hays et al., 1976; Olsen, 1986; Park and Herbert, 1987; Kominz and Bond, 1990; Hinnov and Park, 1998).

Gamma analysis of Kominz and Bond (1990) (see also Bond et al., 1991, 1993; Kominz et al., 1991; Kominz and Bond, 1992; Kominz, 1996; Hinnov and Park, 1998) calculates a thickness–time conversion factor, γ, for each facies in a parasequence, which is the reciprocal of effective sedimentation rate that takes into account effects of compaction and diagenesis and intracycle hiatuses (Yang and Kominz, 1999). Assuming that the effective sedimentation rate of a facies is the same in all parasequences, a group of linear equations may be established for m parasequences in a section:

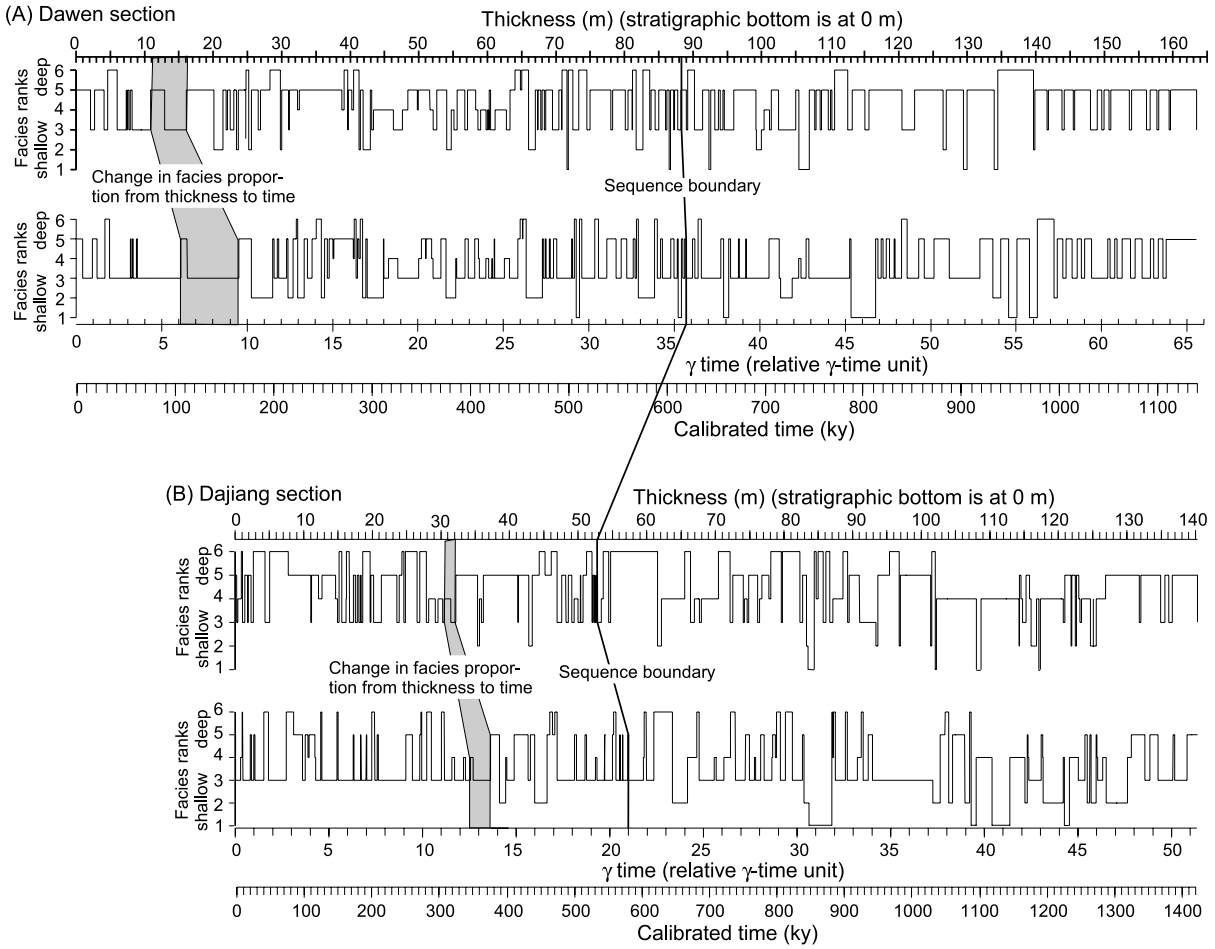

Fig. 4. Facies curves and γ-tuned time series of Dawen (A) and Dajiang (B) sections. Facies-dependent thickness–time conversion using selected γs (Fig. 5) has changed the time proportions of component facies in individual parasequences, as shown in a parasequence correlation (shaded). γ-tuned time series were used for spectral analysis. The first horizontal time axis is in relative γ-time units; the second one is in kyr, as derived from period calibration of spectral peaks.

$$T_{\mathrm{cy},j} = \sum_{i=1}^{n} \gamma_i c_{i,j} \quad j = 1, 2, \ldots, m \tag{1}$$

where n = number of facies in a parasequence, m = number of parasequences ($m \gg n$), i = facies number, j = parasequence number, $T_{\mathrm{cy},j}$ = period of the jth parasequence, c = facies thickness.

The unknowns in Eq. 1 are $T_{\mathrm{cy},j}$ and γ_i. When $T_{\mathrm{cy},j}$ is assumed to be unity for all m parasequences, Eq. 1 becomes an overconstrained linear problem, which is solved by unconstrained least-squares regression to obtain the best-fit γs of the n facies. The assumption that all parasequences have the same duration (i.e. $T_{\mathrm{cy}} = 1$ γ-time unit) is only used in the regression. The best-fit γs minimize the variations in T_{cy} among all m parasequences, but do not produce constant-period parasequences (Kominz and Bond, 1992). A succession of best-fit γs is calculated in iterations using m, $m-1$, ...,n parasequences after removing successively the outlier parasequences in Eq. 1 (see Kominz et al., 1991 for procedure). In the least-squares regression, both γ assumptions are applied to obtain the best-fit γs; but in the removal of successive parasequences, the assumption that all parasequences have equal duration is relaxed (Yang and Kominz, 1999). Finally, the γ

values have the dimension of [(γ-time unit)/(thickness unit)].

The best-fit γs usually stabilize after removal of only a few parasequences (cf. Yang et al., 1995). The stabilized γ values are then used to calculate the duration of facies i in the jth parasequence:

$$t_{i,j} = \gamma_i c_{i,j} \quad (2)$$

and the duration of the entire cyclic section (T) is:

$$T = \sum_{m}^{j=1} \sum_{n}^{i=1} \gamma_i c_{i,j} \quad (3)$$

T includes hiatuses associated with incomplete facies in a parasequence, but not hiatuses represented by entirely missed parasequences (Sadler, 1994).

A facies-dependent (i.e. γ-tuned) time series was converted from a facies curve using Eq. 2. A γ-untuned series was also produced by applying an average γ for all facies, which is calculated by dividing T in Eq. 3 by the thickness of the section. Spectra of γ-tuned and untuned series were calculated to determine periodicity of the section and are compared with each other to determine the effects of tuning via the selected γs, because the γ-untuned spectrum is devoid of the effect of γ tuning.

Gamma analysis has been tested and refined over the last decade through applications on numerous Phanerozoic cyclic successions (e.g. Kominz and Bond, 1990, 1992; Bond et al., 1991, 1993; Kominz et al., 1991; Woronow, 1992; Yang et al., 1995; Kominz, 1996; Hinnov and Park, 1998; Yang and Kominz, 1999). It has been effective in tuning the spectra of ancient cyclic strata where accurate chronostratigraphic time constraints are lacking.

3.2. Results of gamma analysis of the Dawen and Dajiang sections

Prior to gamma analysis, the six facies comprising the Dawen and Dajiang parasequences were combined into two facies, one including the subtidal skeletal packstone, oolitic packstone and grainstone, and calcimicrobial boundstone facies, the other including the intertidal ribbon rock and the supratidal microbial laminite facies. This facies combination was necessary to obtain positive and stable γs in unconstrained least-squares inversion, because many parasequences do not contain all the six component facies (Figs. 2–4; e.g. Yang et al., 1995; Yang and Kominz, 1999).

The best-fit γs of the two combined facies become stable after removal of four parasequences for the Dawen section and only one for the Dajiang section (Fig. 5). The clear separation and stability of the γ values with the successive removal of parasequences suggest that the two combined facies have grossly different sedimentation rates. For both sections, the combined subtidal facies has a smaller γ value (i.e. larger effective sedimentation rate) than the combined intertidal and supratidal facies, although the best-fit γs of Dajiang parasequences are different from those of Dawen parasequences (Fig. 5B). This results from the similar cyclostratigraphic pattern but different detailed lithofacies type and proportions between the closely spaced Dawen and Dajiang sections (Figs. 2 and 3). The Dajiang parasequences formed at the windward edge of the platform and contain more diversified subtidal facies with

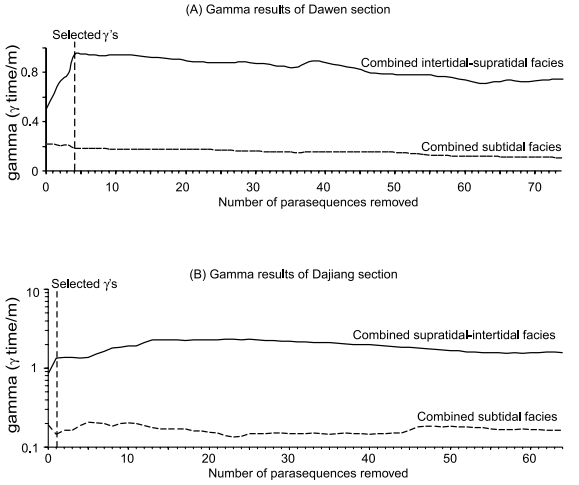

Fig. 5. γ results of Dawen (A) and Dajiang (B) sections. γ values of the combined subtidal and combined intertidal–supratidal facies of the Dawen section stabilize after removal of only a few parasequences. The horizontal axis is the number of parasequences removed in each iteration of least-squares inversion. The selected γs were used to convert facies thickness into time to construct γ-tuned time series of the Dawen and Dajiang sections, respectively.

approximately equal portions of skeletal packstone, oolite, and calcimicrobial boundstone, whereas the Dawen parasequences formed in the platform interior and contain predominantly skeletal packstone in the subtidal facies (Fig. 3). The depositional mechanisms of the three subtidal facies were probably different (e.g. Major et al., 1996; Lehrmann, 1999), causing the differences in absolute values of best-fit γs between the two sections. Combining three subtidal facies into one facies probably exacerbated the differences.

The selected best-fit γs of the combined facies of each section were used to convert the facies curves into γ-tuned time series, wherein the facies curves were non-uniformly stretched into γ-tuned time series (Fig. 4). An average γ for all facies of each section was also used to construct γ-untuned time series, where a facies curve was uniformly stretched into a γ-untuned time series (Fig. 4). All time series are in γ-time units.

3.3. Spectra of γ-tuned and untuned time series of the Dawen section

The spectra of the γ-tuned time series of the Dawen and Dajiang sections were calculated using the multi-window prolate spectral analysis method of Thomson (1982). A prominent spectral peak has a large magnitude in power density. A statistically significant point on the spectrum coincides with a peak of the lower 90% confidence limit and a trough of the upper 90% confidence limit (Figs. 6A and 7A). Only the points that are both statistically significant and on prominent peaks were selected in this study. They were interpreted as representing periodic signals in the time series. Both the Dawen and Dajiang spectra of the γ-tuned time series have several prominent and statistically significant peaks, suggesting quasi-periodicity in the two sections.

The significant peaks were calibrated to obtain their periods in years. The calibration is on a trial-and-error basis (e.g. Yang et al., 1995; Yang and Kominz, 1999). Initially, a peak was arbitrarily assigned to the period of a Milankovitch cycle, and the periods of other peaks were calibrated to it. The periods were then compared with those of major Early Triassic Milankovitch climatic cycles predicted by Berger et al. (1992). Several calibration schemes are possible and the scheme that resulted in a maximum number of Milankovitch peaks on a spectrum was regarded as optimal and is reported here (Fig. 6A).

Four statistically significant and prominent peaks on the Dawen spectrum have periods close to those of long-precessional index (21.2 kyr), short-obliquity (35.8 kyr), and short and long eccentricity (95–131 and 413 kyr) cycles at 247 Ma (Fig. 6A; Berger et al., 1992). Three low-amplitude but statistically significant peaks may also match the Milankovitch peaks. They are the short-precessional index peak (17.7 kyr), the long-obliquity peak (45.3 kyr), and the peak with a period of 9.8–10.4 kyr representing the constructional tone (9.7 kyr) between the short and long-precessional index cycles (Fig. 6A; e.g. Yang et al., 1995). In addition, the peak with a period of 27.5–30.1 kyr between the long-precessional index and the short-obliquity peaks may represent a minor obliquity peak (e.g. Berger, 1977), although it is predicted to occur at 26 kyr for the Early Triassic by Hinnov (2000). Lastly, several distinctive peaks are also present on the γ-untuned spectrum (Fig. 7D). Using the same calibration scheme as for the γ-tuned spectrum, many peaks also fall within major Milankovitch bands.

The γ tuning of the facies curve has concentrated the spectral power into a fewer number of peaks in comparison with the γ-untuned spectrum. Moreover, the close match in period and relative amplitude between peaks on the γ-tuned spectrum and those of the Early Triassic Milankovitch climatic cycles suggests that peritidal cyclic sedimentation of the Dawen section was significantly influenced by Milankovitch climatic forcing.

The spectral character of the Dawen section was further investigated through evolutional spectral analysis of segments of the section. The spectral power shifts toward higher frequency from the lower part to the upper part of the γ-tuned Dawen section (Fig. 6B,C). The evolutional spectral analysis and period calibration used the same parameters and scheme as those for the entire Dawen section. The spectrum of the lower part

contains prominent short and long-obliquity and short-eccentricity peaks, without the precessional index and the long-eccentricity peaks. The spectrum of the upper part, however, contains a prominent long-precessional index peak and low-amplitude but statistically significant short-obliquity, short-precessional index, and constructional-tone peaks. The eccentricity peaks are relatively weak and not well defined in comparison to those of the lower part (Fig. 6B,C). The two spectra indicate that the spectrum of the entire Dawen section (Fig. 6A) appears to be the simple addition of largely mutually exclusive spectral peaks from the lower and upper spectra, with minimal interference among signals of the lower and upper parts of the Dawen section. The spectra also suggest that Milankovitch short-eccentricity and obliquity forcing dominated during the sedimentation of the lower Dawen section, whereas long-precessional index forcing dominated during the sedimentation of the upper Dawen section.

The evolutional spectra differ from that of the entire section for two major reasons. First, the dominant Milankovitch climatic forcing may have changed its character at a location over time and/or at different geographic locations (e.g. Berger, 1988; Berger et al., 1992; deMenocal, 1995; Yang et al., 1995), when the South China Plate migrated across the paleo-equator to the north over several millions of years (Scotese, 1994, 2000). Second, there may have been long-term variations in sedimentation rate during the buildup of GBG, which gamma analysis cannot detect (Hinnov, 2000). Additionally, in both cases, possible interference of individual Milankovitch peaks may change the spectral configuration. Conversely, a seemingly Milankovitch-like spectrum of the entire section could result from interference among non-Milankovitch peaks. Evolutional spectra of the lower and upper parts of the Dawen section indicate minimal long-term spectral interference, provide information on evolving forcing during the course of sedimentation as discussed above, and finally, confirm that the spectral calibration and interpretation of the entire section are reasonable.

The evolutional spectra of segments of the Dawen section confirm the shift of spectral power described above (Fig. 6E). The spectra of the 0–40-m and 20–60-m segments contain prominent short and long-eccentricity peaks and a minor amalgamated short and long-obliquity peak. An abrupt shift to the obliquity occurs in the 40–80-m segment and continues to the 60–100-m segment. The 80–120-m spectrum contains all short and long-eccentricity, amalgamated obliquity, and short and long-precessional index peaks. The other abrupt shift to the long-precessional index occurs in the 100–140-m segment, which also contains significant short-eccentricity power. The complete shift to the precessional index peak occurs in the 120–160-m segment. The low resolution of the evolutional spectra in comparison to those of the entire Dawen section and the lower and upper parts of the Dawen section are expected because the same parameters (e.g. the number of windows) of spectral analysis (Thomson, 1982) were used for short segments of the Dawen section, causing more spectral smoothing (see Section 4). The shift of Milankovitch forcing during the course of cyclic sedimentation of the Dawen section is noteworthy but is expected of typical Milankovitch climatic forcing, as documented in many Plio–Pleistocene records (e.g. Berger, 1988; deMenocal, 1995; Hinnov and Park, 1998). It implies that the dominant depositional mechanisms and controlling factors, which were related to Milankovitch climatic forcings, had changed during the sedimentation of the successive segments of the Dawen section. The changes are reflected by upsection changes in facies proportion and parasequence thickness of the Dawen parasequences (see Section 4).

3.4. Spectra of γ-tuned and untuned time series of the Dajiang section

The γ-tuned spectrum of the entire Dajiang section contains a prominent and statistically significant short-eccentricity peak, and low-amplitude but statistically significant long and short-precessional index and long-eccentricity peaks (Fig. 7A). The scheme of period calibration of the Dajiang spectra is different from that of the Dawen spectra because different best-fit γs were used in con-

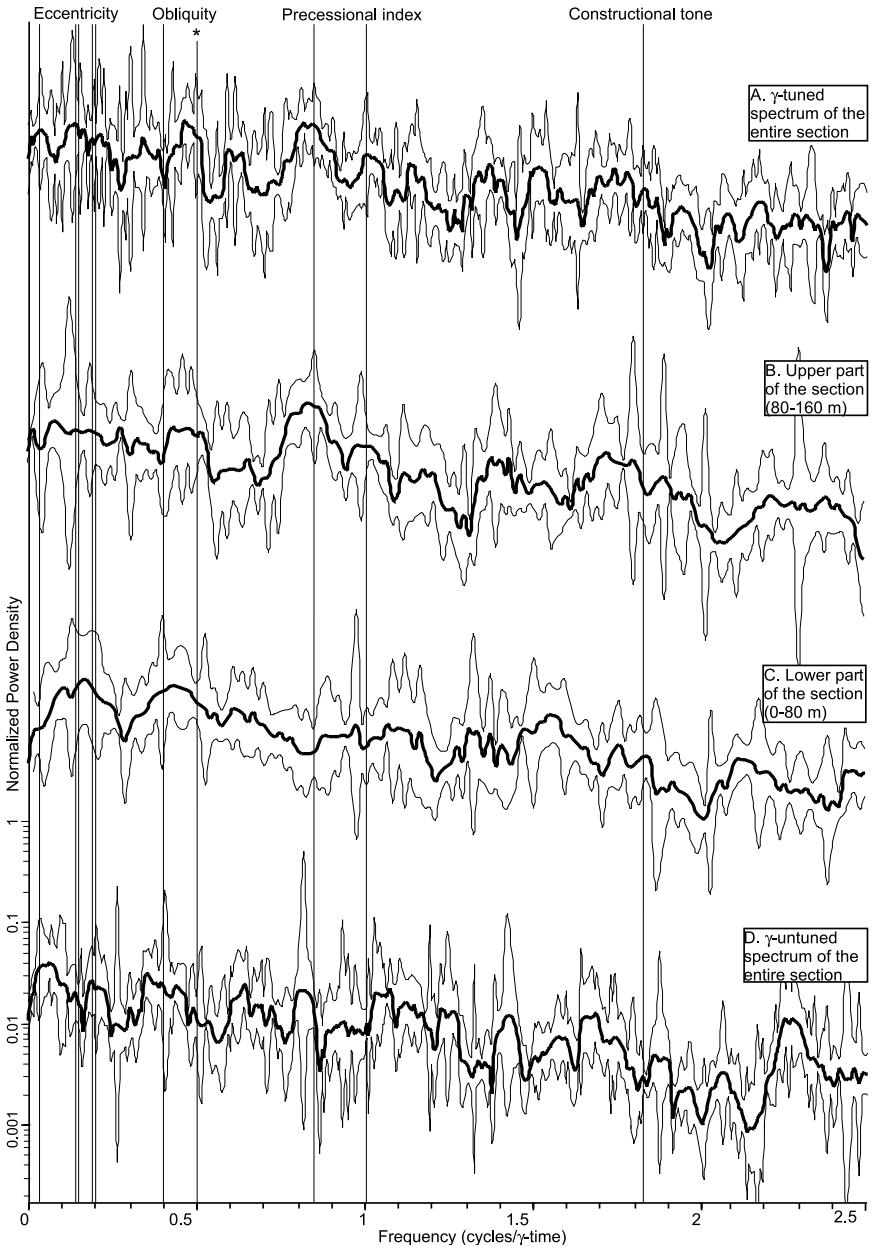

Fig. 6. Spectra of (A) γ-tuned Dawen time series, (B) upper part of γ-tuned series, (C) lower part of γ-tuned series, and (D) γ-untuned Dawen time series. (E) Evolutional spectra of γ-tuned time series. Thick lines are spectra; thin lines below and above the spectral line are lower and upper 90% confidence limits; thin vertical lines are Milankovitch line spectra at 247 Ma (Berger et al., 1992). The period calibration scheme (marked with a star) used in all spectra is (1/0.494 = 35 780 yr, the period of the short-obliquity cycle), which results in one γ-time unit = 17.6 kyr. Nyquist frequency is 20 for all spectra. Spectral power density is normalized for all spectra. Eight windows were used in the spectral analysis (Thomson, 1982). Segments of evolutional spectra are 40 m with a 20-m overlap, as shown in Figs. 2 and 3.

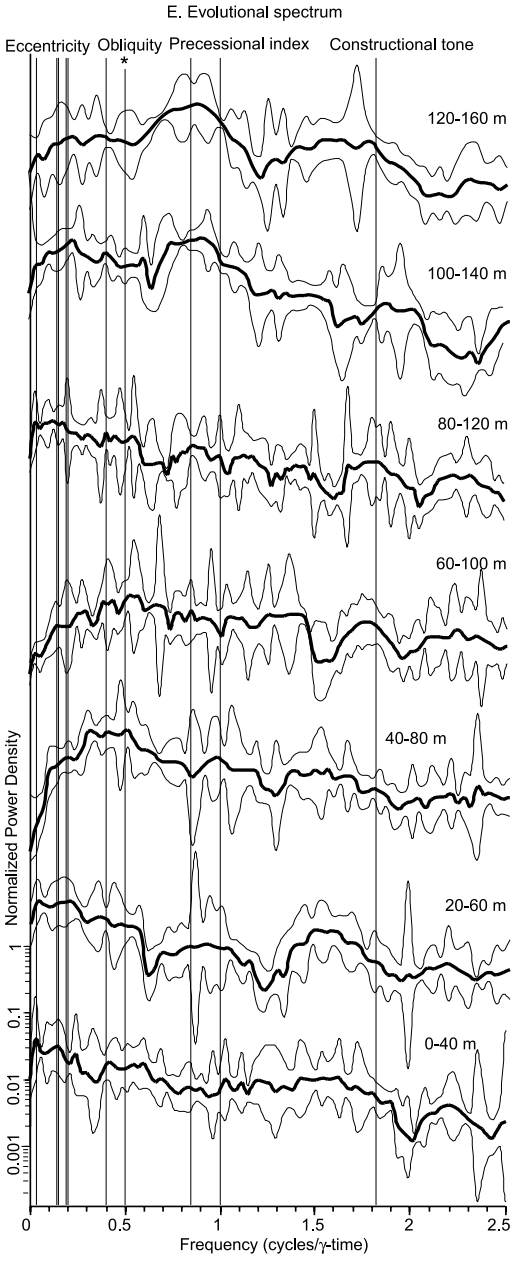

Fig. 6 (*Continued*).

structing the γ-tuned time series (Fig. 3B). The low amplitude of the long-eccentricity peak may be caused by the short thickness of the Dajiang section. A pair of statistically significant and prominent peaks are probably the short and long-obliquity peaks but they have periods slightly longer than those of the long and short-obliquity peaks predicted at 247 Ma by Berger et al. (1992) (Fig. 7A). The slight shift to a lower frequency of the obliquity peaks may indicate mis-tuning by the selected best-fit γs or amalgamation of the short and long-obliquity peaks

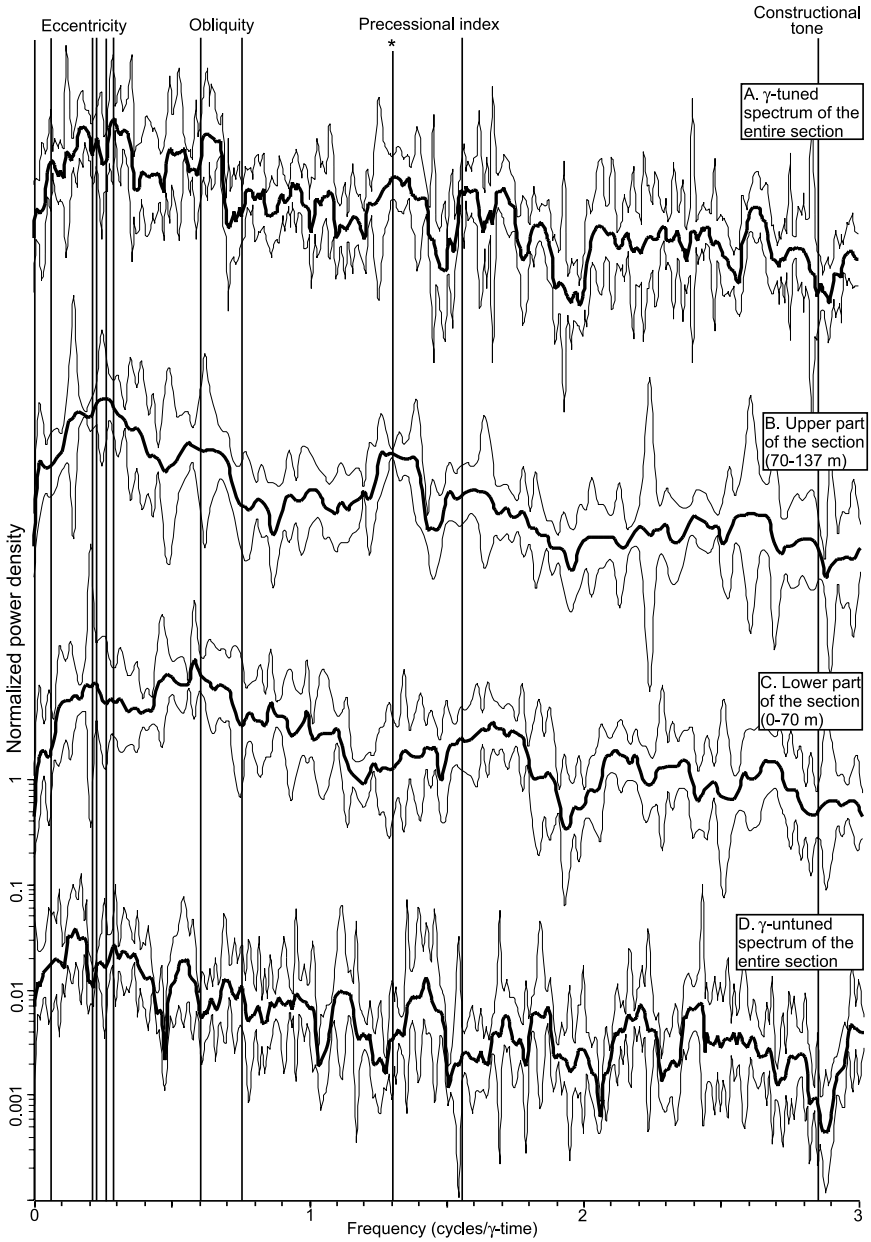

Fig. 7. Spectra of (A) γ-tuned Dajiang time series, (B) upper part of γ-tuned series, (C) lower part of γ-tuned series, and (D) γ-untuned Dajiang time series. (E) Evolutional spectra of γ-tuned time series. The period calibration scheme (marked with a star) used in all spectra is (1/1.304 = 21 248 yr, the period of the long-precessional index cycle), which results in one γ-time unit = 27.7 kyr. Nyquist frequency is 25 for all spectra. Segments of evolutional spectra are 35 m with a 17.5-m overlap, as shown in Figs. 2 and 3. Other parameters, procedures, and explanations are the same as for the Dawen spectra (Fig. 6).

caused by depositional mechanisms, as also seen on the Dawen spectra. A low-amplitude peak of a frequency of about 2.65 may or may not be the constructional tone. The spectral calibration suggests that the Milankovitch climatic forcing probably significantly influenced the formation of Dajiang parasequences, similar to Dawen parasequences. However, the spectral difference between

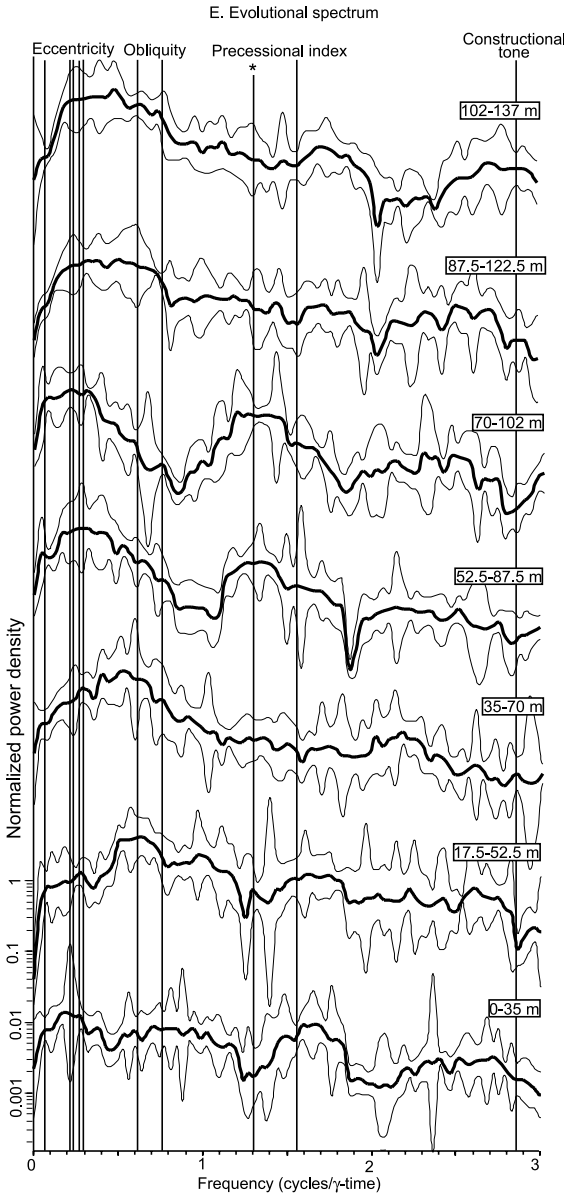

Fig. 7 (*Continued*).

the Dawen and Dajiang sections, mainly the low amplitude of long-precessional index peak and the shift of the short-obliquity peak, suggests that the depositional mechanisms were somewhat different between the platform interior (Dawen) and the windward platform edge (Dajiang) (see Section 4). The quasi-periodicity of the Dajiang record is also suggested by multiple peaks on the γ-untuned pectrum, which have periods close to those of predicted Milankovitch peaks (Fig. 7D).

The spectra of the lower and upper parts of the Dajiang section (Fig. 7B,C) show a decrease in obliquity forcing and an increase in precessional

index and short-eccentricity forcing upsection. This trend is similar to that of Dawen section (Fig. 6B,C). The differences are that, on the spectrum of the upper part of the Dajiang section, the precessional index peak has a small amplitude, the short-eccentricity peak (the destructive tone) has a large amplitude, and the constructional tone is absent.

The shift of Milankovitch climatic forcing during the course of Dajiang sedimentation is displayed on the evolutional spectra (Fig. 7E). The spectral shift of the Dajiang section is similar to that of the Dawen section (Figs. 6E and 7E), with strong obliquity signals in the lower segments but strong precessional-index signals in some of the upper segments. In the Dajiang evolutional spectra, short-eccentricity and short-precessional index peaks are present in the basal 35 m, but the amalgamated obliquity peak is prominent in the 17.5–52.5-m segment. A single broad peak on the 35–70-m spectrum covers the short-obliquity to short-eccentricity band. In the 52.5–87.5-m and 70–102-m segments, the spectral power is concentrated at the short-eccentricity and long-precessional index bands with diminished obliquity power. Upsection, the spectra of the 87.5–122.5-m and 102–137-m segments contain a broad peak covering the short-obliquity to short-eccentricity band, similar to that of the 35–70-m segment. The spectral resolution of Dajiang evolutional spectra is low in comparison to evolutional spectra of the longer segments of the Dawen section. Nevertheless, the general spectral evolution is clear.

The spectral results of the Dawen and Dajiang sections indicate that Milankovitch climatic forcing influenced the cyclic sedimentation on the GBG platform in a greenhouse climate. Furthermore, the evolutional spectra of both sections suggest varying dominance of Milankovitch forcings during the course of sedimentation. Differences between the Dawen and Dajiang spectra and the amalgamated obliquity peak suggest that geologic processes responding to the Milankovitch forcing may have varied between platform interior and windward margin during the course of sedimentation when dominant Milankovitch forcing shifted (discussed below).

4. Discussion

4.1. Sedimentation rate, depositional duration, and stratigraphic completeness

The period calibration of spectral peaks to the Milankovitch cycle periods assigned absolute time to the γ-time units of the Dawen and Dajiang series. A unit of γ-time of the Dawen series is equal to 17.6 kyr and that of the Dajiang series is 27.7 kyr (Table 1). Then, the sedimentation rates of the two combined facies, which are the reciprocals of selected best-fit γs, were calculated as 6.0 and 2.7 cm/kyr for the combined intertidal–supratidal facies and 30.7 and 24.6 cm/kyr for the combined subtidal facies for the Dawen and Dajiang parasequences, respectively (Table 1).

Subsequently, the duration represented by the total thickness of all parasequences in Dawen and Dajiang sections was calculated using Eq. 3 as 1139 and 1423 kyr, respectively (Table 1). The duration is the time represented by complete and partially eroded parasequences (Sadler, 1994), excluding the hiatal time represented by completely missing parasequences, which were not used in gamma analysis (Yang and Kominz, 1999). Thus, the duration can be regarded approximately as the duration of deposition of a section. On the other hand, the total duration of the Dawen or Dajiang section, including time represented by both rocks and hiatal surfaces, was estimated as 2.125 or 3 Myr, with a potential range from a minimum of 1.55 Myr to a maximum of 3.6 Myr according to recent geochronologic constraints (Bowring et al., 1998; Mundil et al., 2001; Martin et al., 2001; see discussion in Section 2.3). The ratio between the depositional duration and the chronostratigraphically estimated total duration represents the stratigraphic completeness of a section (cf. Sadler, 1981). Thus, corresponding to the two estimated age dates and maximum to minimum ages considering errors, the stratigraphic completeness of the Dawen section is estimated to be 38–54%, with a minimum of 32% and maximum of 73%, and that of the Dajiang section is 47–67%, with a minimum of 40% and a maximum of 92%. Last, the average sedimentation rate of a section was calculated by

Table 1
Sedimentation rate, depositional duration, and stratigraphic completeness of the Dawen and Dajiang sections based on spectral calibration

	Unit γ time (kyr)	Selected γs (γ time/m)	Effective sedimentation rate (cm/kyr)	Average sedimentation rate (cm/kyr)	Depositional duration (kyr)	Stratigraphic completeness (%[a])
Dawen section	17.6	0.95 (combined intertidal and supratidal facies) 0.18 (combined subtidal facies)	6.0 (combined intertidal and supratidal facies) 30.7 (combined subtidal facies)	7.0	1139	38–54 (32–73)
Dajiang section	27.7	1.34 (combined intertidal and supratidal facies) 0.15 (combined subtidal facies)	2.7 (combined intertidal and supratidal facies) 24.6 (combined subtidal facies)	9.9	1423	47–67 (40–92)

[a] The range of stratigraphic completeness corresponds to the two estimates of mean duration of the Olenekian Stage (3 and 2.125 Myr). The range given in parentheses corresponds to the maximum and minimum estimated duration of the Olenekian Stage (3.6 and 1.55 Myr). See text for discussion on stratigraphic completeness and age estimate.

dividing the depositional duration by the total thickness of a section. The rate is 7.0 cm/kyr for the Dawen section and 9.9 cm/kyr for the Dajiang section (Table 1).

The sedimentation rate of the combined subtidal facies is about five and eight times greater than that of the combined intertidal–supratidal facies for the Dawen and Dajiang sections, respectively. These rates and the average sedimentation rates are within the range of documented peritidal carbonate sedimentation rates of modern and ancient analogs (e.g. Hallock and Schlager, 1986; Kukal, 1990; Enos, 1991; Sadler, 1994). This suggests that: (1) the gamma analysis successfully differentiated the relative time represented by the subtidal and intertidal–supratidal facies; (2) the facies-dependent thickness–time conversion is more accurate than the thickness-proportional conversion; and (3) the period calibrations of Dawen and Dajiang spectra are valid, yielding reasonable and consistent sedimentation rates, even though the best-fit γs for the two sections are different. However, we caution against citing the exact values of sedimentation rate and stratigraphic completeness, because they were derived from γ estimates and chronostratigraphic time estimates with variable uncertainties. The values are likely only reliable in the general trend and order of magnitude (cf. Sadler, 1981, 1994; also see below).

In addition, the Dawen and Dajiang sections, located 3 km apart, have comparable depositional durations, suggesting that the period calibrations are valid. It may seem inconsistent that the Dawen section has a shorter depositional duration than the Dajiang section since the Dawen section has more parasequences (82 vs. 66) and is thicker than the Dajiang section (164 vs. 137 m). We explain this apparent inconsistency as follows. First, the primary function of the best-fit γs is tuning the spatial facies curves; thus, the sedimentation rates and the depositional durations should not be regarded as exact values (Kominz and Bond, 1990, 1992; Kominz, 1996; Yang and Kominz, 1999). Second, the depositional duration of a parasequence depends mainly on the proportions of facies with unique sedimentation rates. Thus, two parasequences of equal thickness may have different durations if one parasequence contains a larger proportion of the facies with a low sedimentation rate than the other parasequence. Finally, the multiple peaks on the Dawen and Dajiang spectra indicate that the parasequences do not have equal duration (see also next section). Moreover, the variety of subtidal facies in the Dawen and Dajiang parasequences probably do not have precisely the same sedimentation rates, although they were combined and assigned with the same sedimentation rate in gamma analysis. This discrepancy would also contribute to the difference between the estimated depositional durations of the two sections. There must have been additional

factors affecting the depositional duration of Dawen and Dajiang sections. Above all, the depositional durations of the Dawen and Dajiang sections may be regarded as roughly equal.

The stratigraphic completeness of the Dawen section (32–73%) and Dajiang section (40–92%) is much higher than those estimated for other shallow-marine and non-marine records, which are commonly less than 20% (e.g. Sadler, 1981, 1994; Wilkinson et al., 1992; Yang and Kominz, 1999; cf. Sadler, 1999). The relatively high stratigraphic completeness of the two sections may be associated with the greenhouse climate, when large sea-level fluctuations were absent (see also Sadler, 1994). Carbonate platform records formed during periods of continental glaciation are likely to be less continuous than those formed during periods of non-glaciation (e.g. Wilkinson et al., 1992; Sadler, 1994; Read, 1995; Yang et al., 1995), because large sea-level fluctuations would have repeatedly exposed the carbonate platform to cause abundant erosional and non-depositional hiatuses and missed beats (cf. Goldhammer et al., 1990). Supratidal facies are minimal in the Dawen and Dajiang sections (Fig. 3), suggesting little subaerial exposure time, resulting in the relatively high stratigraphic completeness of the two records.

4.2. Sedimentary expressions of Milankovitch climatic signals in Dawen and Dajiang strata

The link between Milankovitch climatic forcing and cyclic sedimentation is largely a 'black box' due to the complex interplay of many climatic, oceanic, biologic, tectonic, and sedimentary processes that control sedimentation. The evolving Milankovitch climatic signals in the GBG records serve as a starting point to examine the link. The depositional mechanisms of cyclic peritidal carbonate sedimentation on the GBG in a greenhouse climate have been the subject of ongoing research (e.g. Lehrmann and Goldhammer, 1999; Lehrmann et al., 2001; Yang and Lehrmann, 2001; Yang et al., 2002). The following discussion briefly explores the sedimentary expressions of Milankovitch climatic signals in the GBG records.

4.2.1. Dawen section

The strong obliquity and short-eccentricity signals in the lower part of the Dawen section suggest two orders of cyclicity (Fig. 6C). However, they are not strictly hierarchical because orbital eccentricity and obliquity are physically independent, whereas the precessional index is modulated by the eccentricity (Berger, 1977, 1988; Berger et al., 1992; cf. Liu et al., 2000). Eccentricity is dominant in the 0–40-m and 20–60-m segments, whereas obliquity is dominant in the 40–80-m segment (Fig. 6E). This character is reflected in the time series and facies curve (Fig. 4A). The 0–60-m segment contains a mixture of thick/long and moderately thick/moderately long parasequences (thick or thin denotes interval in space, long or short denotes interval in time). Some of the longer parasequence sets contain thin/short parasequences and are probably bundles of short parasequences. If eccentricity signals arise from destructive interference of the precessional index, the lack of power in the precessional index band suggests that eccentricity came to dominate the precessional index carrier through some non-linear climatic and geologic interactions (e.g. Ripepe and Fischer, 1991; deMenocal, 1995). The 40–80-m segment, on the other hand, contains predominantly parasequences of approximately equal thickness/duration and lacks thick/long parasequences (Fig. 4A). The correlation between the thickness and duration of parasequences and the calibrated Milankovitch periods implies that the thick/long parasequences are short-eccentricity cycles, the moderately thick/moderately long parasequences are obliquity cycles, and the thin/short parasequences are precessional-index cycles.

A one-on-one correlation of the GBG parasequences, their thickness, duration, and facies composition with Milankovitch cycles is tentative at best. First, the multiple spectral peaks indicate that the Dawen series is quasi-periodic, as are the Milankovitch climatic series. Even the period of a specific Milankovitch cycle, be it short eccentricity, obliquity, or precessional index, varies over several to 10s of kyr (Yang, 1996; Hinnov, 2000). Second, the algorithm and parameters used in spectral analysis affect the precision of the periods of spectral peaks (Thomson, 1982; Brace-

well, 1986; e.g. Yang et al., 1995). Last but not least, allogenic and autogenic geologic processes other than Milankovitch climatic forcing affect cyclic sedimentation. For example, stratigraphic incompleteness caused by the erosional and non-depositional hiatuses and inaccuracy in thickness–time conversion affect spectral analysis (Sadler, 1994; Yang and Kominz, 1999). These processes must also have mixed their signals with Milankovitch signals in the GBG records.

The upper part of the Dawen section has an exceptionally strong long-precessional index signal (Fig. 6B). The destructive tone of the precessional index signals, i.e. eccentricity, is weak but the constructional tone is conspicuous. The presence of thick/long and very thin/very short parasequences in the 90–125-m segment reflects the spectral character of co-existing precessional index and short-eccentricity (Figs. 4A and 6E). On the other hand, the thin but approximately equal-thickness/duration parasequences in the 120–160-m segment reflect the dominance of precessional index with a minor constructional tone peak (Fig. 6E).

The spectrum of the 60–100-m segment of the Dawen section has a broad peak centered on the obliquity band. It is the transition from the lower obliquity-dominated spectrum to the upper precessional-index-dominated spectra (Fig. 6E). The spectral transition is reflected in the facies curve and time series (Fig. 4A), where thin/short parasequences mix with moderately thick/moderately long parasequences in this segment. The absence of sharp spectral peaks may be the result of mixing of obliquity in the lower part and the precessional index in the upper part of the segment or unmodeled sedimentation rate changes. This segment covers the stratigraphic turning point from the upper HST to the lower TST across the SB (Figs. 2A and 4A). The correlation between spectral and stratigraphic transition may indicate an unknown cause–effect relationship between Milankovitch climatic forcing and cyclic sedimentation.

4.2.2. *Dajiang section*

The obliquity signals are dominant in the lower part of the Dajiang section (Fig. 7C). In detail, The 0–35-m spectrum has clearly defined short-precessional index and short-eccentricity peaks (Fig. 7E), as reflected by the mixture of thick/long parasequences and thin/short parasequences on the facies curve and time series (Fig. 4B). Upsection, the obliquity becomes dominant in the 17.5–52.5-m and 35–70-m segments, as reflected by many parasequences of similar duration in these segments (Fig. 4B). The spectral character of evolutional spectra of the lower Dajiang section is similar to those of the lower Dawen section (Figs. 6C,E and 7C,E). For example, the 17.5–52.5-m segment of the Dajiang series correlates stratigraphically with the 60–90-m segment of the Dawen series (Fig. 2) and both segments are dominated by obliquity (Figs. 6E and 7E). In addition, the spectra of the segments covering the SB (35–70 m in the Dajiang series, 60–100 m in the Dawen series) are both poorly defined and signify a spectral transition associated with the SB, characterized by a shift from obliquity to precessional index and eccentricity.

The spectral shift upsection across the SB is marked by prominent short-eccentricity and long-precessional index peaks on the spectra of the 52.5–87.5-m and 70–102-m segments (Fig. 7E). This shift corresponds to the occurrence of thick/long parasequences and, for the first time, supratidal microbial laminites (Figs. 3B and 4B). Upsection, the spectra of the 87.5–122.5-m and 102–137-m segments are characterized by a broad low-frequency peak spanning the obliquity and short-eccentricity band, indicating a return of obliquity forcing and absence of precessional index forcing (Fig. 7E). The spectral character is reflected by the mixture of thick/long and moderately thick/moderately long parasequences in the two segments (Fig. 4B).

There are similarities and dissimilarities in spectral character between the upper Dajiang and upper Dawen sections. The similarity is the presence of long and short-precessional index peaks. This may be related to the first occurrence of supratidal microbial laminite in both sections (Figs. 4, 6B and 7B). The spectra of the 52–87.5-m and 70–102-m segments of the Dajiang section are also similar to the spectrum of the 100–140-m segment of the Dawen section. The

major dissimilarity is the absence of a strong long-precessional index signal but the presence of a strong short-eccentricity signal in the upper Dajiang section. In detail, the dissimilarity originates from the different spectral peaks between the uppermost Dajiang and Dawen sections. The 120–160-m spectrum of the Dawen section is dominated by a single precessional index peak, whereas the 87.5–122.5-m and 102–137-m spectra of the Dajiang section are dominated by a broad peak spanning the obliquity and short-eccentricity bands (Figs. 6E and 7E). The difference corresponds to different facies compositions between the uppermost parts of the two sections (Fig. 3A,B). Subtidal skeletal packstone and intertidal laminated lutite dominate the uppermost Dawen section, whereas diverse subtidal oolite and skeletal packstone and intertidal ribbon rocks and lutite dominate the uppermost Dajiang section. The correlation between spectral difference and different facies associations at the platform interior and windward platform margin suggests different depositional/recording mechanisms of Milankovitch climatic signals at the two localities during the course of sedimentation.

4.3. Mechanisms of Milankovitch climatic control on peritidal cyclic carbonate sedimentation

The spectral evidence linking Milankovitch climatic forcing and parasequence characteristics provides clues for interpreting the mechanisms of cyclic sedimentation on the GBG in a greenhouse climate in an equatorial mid-ocean setting. A thorough exploration requires more data (e.g. geochemical and paleontologic) in addition to those presented above. Only a few speculations are presented here.

A close examination of facies composition indicates that strong obliquity signals are present in segments containing abundant oolites and thin/short parasequences, such as the 40–80-m and 60–100-m segments in the Dawen section (Figs. 2A, 3A and 6E) and the 17.5–52.5-m, 87.5–122.5-m, and 102–137-m segments in the Dajiang section (Figs. 2B, 3B and 7E). Formation, distribution, and deposition of oolitic sediments are closely related to climatic and oceanic conditions that affect the energy and water chemistry of the windward platform margin. For example, the frequency and strength of tropical storms would affect the extent and thickness of oolite spill-over lobes into the platform interior (Fig. 1C). Plate reconstructions place the Dajiang section of the GBG at 12°N latitude facing N45°E into the northeast trade winds (Fig. 1; Kutzbach et al., 1990; Crowley, 1994; Scotese, 1994, 2000). Thus, obliquity forcing may have been transferred to the sedimentary record via equatorial atmospheric circulation (cf. Crowley, 1994).

Variations in carbonate productivity in the subtidal factory could have affected carbonate sediment supply in the shallow subtidal, intertidal, and supratidal environments on the GBG platform (Yang et al., 2002). The slowly recovering biota and low bio-diversity of the superanoxic ocean in the Early Triassic (cf. Stanley, 1988; Wignall and Hallam, 1992; Isozaki, 1994; Knoll et al., 1996) makes this mechanism attractive. Periodic flooding of the subtidal carbonate factory by anoxic ocean water could have caused fluctuations in carbonate productivity. The flooding could have been induced by periods of intense upwelling driven by hemispheric deep-water circulation.

In addition, low-amplitude sea-level fluctuations, which certainly had caused changes in accommodation space on the GBG platform, may have aided anoxic flooding in causing carbonate productivity changes. Sea-level fluctuations are indicated by the presence of supratidal microbial laminites, albeit few, in the sections and the correlation among parasequences, parasequence sets, and depositional sequences between the two sections (Lehrmann et al., 2001; Yang and Lehrmann, 2001). Non-glacial global and regional sea-level changes of several meters can be caused, for example, by variations in continental water storage, which were induced by Milankovitch climatic forcing (Jacobs and Sahagian, 1993).

The spectral shift in Milankovitch climatic forcing suggests, on the other hand, that no one mechanism dominated through the entire course of sedimentation. The latitudinal position and, perhaps, the orientation of the GBG platform may have determined that the platform was sub-

ject to varying climatic and oceanic conditions induced by different Milankovitch forcing mechanisms (e.g. Kutzbach et al., 1990). Paleomagnetic data indicated that the Yangtze Block migrated northward from the paleo-equator in the Late Permian to 12°N at the end of the Olenekian and experienced a 45° clockwise rotation (Fig. 1A,B; Enkin et al., 1992; Van der Voo, 1993; P. Montgomery, personal communication, 2002). If the evolving Milankovitch signals in the GBG records were mainly caused by an estimated 6–7° northward plate movement during the Olenekian, the latitudinal climatic gradient in the eastern Tethys must have been very steep, conforming with a similar interpretation from the low-latitude continental record in Late Triassic western Pangea (Kent and Olsen, 2000).

The other possible scenario is that, assuming the amount of plate movement is insignificant during the Olenekian, the evolving Milankovitch climatic forcing may have been caused mainly by dynamic changes of global atmospheric and oceanic conditions. Temporal changes of dominant Milankovitch climatic forcing at a given locality were documented in continental northwestern Africa in the Plio–Pleistocene (e.g. deMenocal, 1995), and should have been common in the geological records (Berger, 1988; see Hinnov and Park, 1998; Meyers et al., 2001; Palike et al., 2001 for more examples) because of complex interaction of atmospheric and oceanic systems (e.g. Crowley, 1994). The above speculations on depositional mechanisms and paleoclimatic changes suggest that depositional processes and mechanisms, other than sea-level fluctuations, may have played a major role in cyclic sedimentation on the GBG.

5. Conclusions

Milankovitch signals were calibrated on the spectra of the Dawen and Dajiang peritidal cyclic carbonate sections deposited on an isolated carbonate platform, the GBG, South China, during the Early Triassic period of greenhouse climate, with prominent short-eccentricity, short-obliquity, and long-precessional index peaks.

The sedimentation rates of subtidal and intertidal–supratidal facies were estimated on the basis of period calibration of the Dawen and Dajiang spectra. The sedimentation rate of subtidal facies ranges from 30.7 to 24.6 cm/kyr and that of intertidal–supratidal facies ranges from 6.0 to 2.7 cm/kyr. The estimated depositional duration ranges from 1139 to 1423 kyr. The stratigraphic completeness, which is the ratio between the depositional duration and the chronostratigraphically estimated total duration, was estimated as 32–92%, suggesting that greenhouse peritidal records are more complete than icehouse peritidal records.

Evolutional spectra of segments of the Dawen and Dajiang sections indicate that Milankovitch climatic forcing varied among short-eccentricity, obliquity, and long-precession during the course of sedimentation. The spectral variation is reflected in the variations in parasequence thickness, duration, and facies composition. Milankovitch climatic forcing greatly influenced the peritidal cyclic sedimentation on the GBG. The evolving Milankovitch signals and the dissimilarities between Dawen and Dajiang spectra suggest that a variety of climatic, oceanic, and geologic processes and mechanisms may have been operating at the platform interior and windward platform margin during the course of cyclic sedimentation. One mechanism, for example, could be the variation in subtidal carbonate productivity as induced by upwelling and flooding of anoxic ocean water onto the platform, low-amplitude non-glacial sea-level fluctuations, variations in frequency and strength of tropical storms, and/or latitudinal plate movement and rotation. This study provides clues for future research on the mechanisms of climatic forcing on peritidal cyclic sedimentation in a greenhouse climate.

Acknowledgements

M. Kominz provided the computer codes for gamma and spectral analyses. Reviews by P. Wignall and, especially, L. Hinnov have greatly improved the science and readability of the manuscript. D.J.L. was supported by grants from the

National Science Foundation (under Grant No. EAR-9804835) and the Petroleum Research Fund of the American Chemical Society (under Grant No. ACS-PRF 33122-B8).

References

Barrell, J., 1917. Rhythms and the measurements of geologic time. Geol. Soc. Am. Bull. 28, 745–904.

Berger, A., 1977. Support for the astronomical theory of climatic change. Nature 269, 44–45.

Berger, A., 1988. Milankovitch theory and climate. Rev. Geophys. 26, 624–657.

Berger, A., Loutre, M.F., Laskar, J., 1992. Stability of the astronomical frequencies over the Earth's history for paleoclimate studies. Science 255, 560–566.

Berner, R.A., 1991. A model for atmospheric CO_2 over Phanerozoic time. Am. J. Sci. 291, 339–376.

Bond, G.C., Kominz, M.A., Beavan, J., 1991. Evidence for orbital forcing of Middle Cambrian peritidal cycles: Wah Wah range, south-central Utah. In: Franseen, K., Watney, W.L., Kendall, C.G.St.C., Ross, W. (Eds.), Sedimentary Modeling: Computer Simulations and Methods for Improved Parameter Definition. Kansas Geol. Surv. Bull. 233, 293–317.

Bond, G.C., Devlin, W.J., Kominz, M.A., Beavan, J., McManus, J., 1993. Evidence of astronomical forcing of the Earth's climate in Cretaceous and Cambrian times. Tectonophysics 222, 277–294.

Bottjer, D.J., Schubert, J.K., 1997. Paleoecology of Lower Triassic marine carbonates in the southwestern USA. Brigham Young Univ. Res. Lett. 42, 15–18.

Bowring, S.A., Erwin, D.H., Jin, Y.G., Martin, M.W., Davidek, K., Wang, W., 1998. U/Pb zircon geochronology and tempo of the end-Permian mass extinction. Science 280, 1039–1045.

Bracewell, R.N., 1986. The Fourier Transform and its Application, 2nd edn. McGraw-Hill, New York, 450 pp.

Broglio Loriga, C., Neri, C., Posenato, R., 1986. The Lower Triassic of the Dolomites and Cadore. IGCP Project 203, Brescia, Guidebook, pp. 29–34.

Broglio Loriga, C., Coczan, F., Janos, H., Lenner, K., Neri, C., Scheffer, A.O., Posenato, R., Szabo, I., Makk, A.T., 1990. The Lower Triassic of the Dolomites (Italy) and the Transdanubian Mid-mountains (Hungary) and their correlation. Mem. Sci. Geol. 42, 41–103.

Crowley, T.J, 1994. Pangean climates. In: Klein, G.D. (Ed.), Pangea: Paleoclimate, Tectonics, and Sedimentation during Accretion, Zenith and Breakup of a Supercontinent. Geol. Soc. Am. Spec. Paper 288, Boulder, CO, pp. 25–40.

Crowley, T.J., Kim, K.-Y., Mengel, J.G., Short, D.A., 1992. Modeling 100,000-year climate fluctuations in pre-Pleistocene time series. Science 255, 705–707.

deMenocal, P.B., 1995. Plio-Pleistocene African climate. Science 270, 53–59.

Enkin, R.J., Yang, Z., Chen, Y., Courtillot, V., 1992. Paleomagnetic constraints on the geodynamic history of the major blocks of China from the Permian to the present. J. Geophys. Res. B 97, 13953–13989.

Enos, P., 1991. Sedimentary parameters for computer modeling. In: Franseen, E.K., Watney, W.L., Kendall, C.G.St.C., Ross, W. (Eds.), Sedimentary Modeling; Computer Simulations and Methods for Improved Parameter Definition. Kansas Geol. Surv. Bull. 233, 63–100.

Enos, P., 1995. Permian of China. In: Scholle, P.A., Peryt, T.M., Ulmer-Scholle, D.S. (Eds.), The Permian of Northern Pangea, vol. 2. Springer, Berlin, pp. 225–256.

Fischer, A.G., 1964. The Lofer cyclothems of the Alpine Triassic. Kansas Geol. Surv. Bull. 169, 107–149.

Flügel, E., 1982. Evolution of Triassic reefs: current concepts and problems. Facies 6, 297–328.

Flügel, E., Stanley, G.D., Jr., 1984. Reorganization, development and evolution of post-Permian reefs and reef organisms. Palaeontographica Americana 54, 177–186.

Frakes, L.A., Francis, J.E., Syktus, J.I., 1992. Climate Models of the Phanerozoic: The History of Earth's Climate over the past 600 Million Years. Cambridge University Press, Cambridge, 274 pp.

Goldhammer, R.K., Dunn, P.A., Hardie, L., 1990. Depositional cycles, composite sea-level changes, cycle stacking patterns, and the hierarchy of stratigraphic forcing: Examples from Alpine Triassic platform carbonates. Geol. Soc. Am. Bull. 102, 535–562.

Goldhammer, R.K., Lehmann, P.J., Dunn, P.A., 1993. The origin of high-frequency platform carbonate cycles and third-order sequences (Lower Ordovician El Paso Group, West Texas): constraint from outcrop and stratigraphic modeling. Journal of Sedimentary Research 63, 318–359.

Guangxi Bureau of Geology and Mineral Resources, 1985. Regional geology of Guangxi. Geological Memoirs 1(6) (in Chinese, English summary; geologic map scale 1:500,000).

Guizhou Bureau of Geology and Mineral Resources, 1987. Regional geology of Guizhou Province. Geological Memoires 1(6) (in Chinese, English summary; geologic map scale 1:500,000).

Hallock, P., Schlager, W., 1986. Nutrient excess and the demise of coral reefs and carbonate platforms. Palaios 1, 389–398.

Harland, W.B., Armstrong, R.L., Cox, A.V., Craig, L.E., Smith, A.G., Smith, D.G., 1989. A Geologic Time Scale. Cambridge University Press, 263 pp.

Hays, J.D., Imbrie, J., Shackleton, N.J., 1976. Variations in the Earth's orbit: Pacemaker of the ice ages. Science 194, 1121–1132.

Hinnov, L.A., 2000. New perspectives on orbitally forced stratigraphy. Annu. Rev. Earth Planet. Sci. 28, 419–475.

Hinnov, L.A., Goldhammer, R.K., 1991. Spectral analysis of the Middle Triassic Latemar Limestone. J. Sediment. Petrol. 61, 1173–1193.

Hinnov, L.A., Park, J., 1998. Detection of astronomical cycles in the stratigraphic record by frequency modulation (FM) analysis. J. Sediment. Res. 68B, 524–539.

Isozaki, Y., 1994. Superanoxia across the Permo-Triassic boundary: Record in accreted deep-sea pelagic chert in Japan. In: Embry, A.F., Beauchamp, B., Glass, D.J. (Eds.), Pangea: Global Environments and Resources. Can. Soc. Pet. Geol., Calgary, AB, 805–812.

Isozaki, Y., 1997. Permo-Triassic boundary superanoxia and stratified superocean: Records from the lost deep sea. Science 276, 235–238.

Jacobs, D.K., Sahagian, D.L., 1993. Climate induced fluctuations in sea level during non-glacial times. Nature 361, 710–712.

Kent, D.V., Olsen, P.E., 2000. Magnetic polarity stratigraphy and paleolatitude of the Triassic-Jurassic Blomidon Formation in the Fundy basin (Canada): implications for Early Mesozoic tropical climate gradients. Earth Planet. Sci. Lett. 179, 311–324.

Kerans, C., Tinker, S., 1997. Sequence Stratigraphy and Characterization of Carbonate Reservoirs. SEPM Short Course Notes 40, Tulsa, OK.

Klimetz, M.P., 1983. An outline of the Mesozoic plate evolution of eastern China. Tectonics 2, 139–166.

Knoll, A.H., Bambach, R.K., Canfield, D.E., Grotzinger, J.P., 1996. Comparative Earth history and the Late Permian mass extinction. Science 273, 452–457.

Kominz, M.A., 1996. Whither cyclostratigraphy? Testing the gamma method on Upper Pleistocene deep-sea sediments North Atlantic Deep Sea Drilling Project Site 609. Paleoceanography 11, 481–504.

Kominz, M.A., Bond, G.C., 1990. A new method of testing periodicity in cyclic sediments-application to the Newark Supergroup. Earth Planet. Sci. Lett. 98, 233–244.

Kominz, M.A., Bond, G.C., 1992. Documenting the reliability and utility of the γ method as applied to cyclic sections using forward modeling. Earth Planet. Sci. Lett. 113, 449–457.

Kominz, M.A., Beavan, J., Bond, G.C., McManus, J., 1991. Are cyclic sediments periodic? Gamma analysis and spectral analysis of Newark Supergroup lacustrine strata. In: Franseen, K., Watney, W.L., Kendall, C.G.St.C., Ross, W. (Eds.), Sedimentary Modeling: Computer Simulations and Methods for Improved Parameter Definition. Kansas Geol. Surv. Bull. 233, 319–334.

Kukal, Z., 1990. The Rate of Geological Processes. Earth-Science Reviews vol. 28, Elsevier, 259 pp.

Kutzbach, J.E., 1994. Idealized Pangea climates: Sensitivity to orbital changes. In: Klein, G.D. (Ed.), Pangea: Paleoclimate, Tectonics, and Sedimentation during Accretion, Zenith and Breakup of a Supercontinent. Geol. Soc. Am. Spec. Paper 288, Boulder, CO, 41–56.

Kutzbach, J.E., Guetter, P.J., Washington, W.M., 1990. Simulated circulation of an idealized ocean for Pangaean time. Paleoceanography 5, 299–317.

Lehrmann, D.J., 1993. The Great Bank of Guizhou: birth evolution and death of an isolated Triassic carbonate platform, Guizhou Province, south China. Ph.D. dissertation, University of Kansas, Lawrence, KS, 457 pp.

Lehrmann, D.J., 1999. Early Triassic calcimicrobial mounds and biostromes of the Nanpanjiang basin, south China. Geology 27, 359–362.

Lehrmann, D.J., Goldhammer, R.K., 1999. Secular variation in facies and parasequence stacking patterns of platform carbonates: a guide to application of the stacking patterns technique in strata of diverse ages and settings. In: Harris, P.M., et al. (Eds.), Recent Advances in Carbonate Sequence Stratigraphy; Applications to Reservoirs, Outcrops and Models. SEPM Spec. Publ. 62, 187–226.

Lehrmann, D.J., Wei, J., Enos, P., 1998. Controls on facies architecture of a large Triassic carbonate platform: The Great Bank of Guizhou, Nanpanjiang Basin, South China. J. Sediment. Res. 68, 311–326.

Lehrmann, D.J., Yang, W., Wei, J., Yu, Y., Xiao, J., 2001. Lower Triassic peritidal cyclic limestone: an example of anachronistic carbonate facies from the Great Bank of Guizhou, Nanpanjiang Basin, Guizhou province, South China. Paleogeogr. Paleoclimatol. Paleoecol. 173, 103–123.

Li, Z.X., 1998. Tectonic history of the major East Asian lithospheric blocks since the mid-Proterozoic - a Synthesis, in mantle dynamics and plate interactions in East Asia. AGU Geodyn. 27, 221–243.

Liu, Z., Kutzbach, J., Wu, L., 2000. Modeling climate shift of El Nino variability in the Holocene. Geophys. Res. Lett. 27, 2265–2268.

Major, R.P., Bebout, D.G., Harris, P.M., 1996. Recent evolution of a Bahamian ooid shoal: effects of Hurricane Andrew. Geol. Soc. Am. Bull. 108, 168–180.

Martin, M.W., Lehrmann, D.J., Bowring, S.A., Enos, P., Ramezani, J., Wei J., Zhang J., 2001. Timing of Lower Triassic carbonate bank buildup and biotic recovery following the end-Permian extinction across the Nanpanjiang Basin, South China. Geol. Soc. Am., Abstracts with Programs 33, A-201.

Meyers, S.R., Sageman, B.B., Hinnov, L.A., 2001. Integrated quantitative stratigraphy of the Cenomanian-Turonian Bridge Creek Limestone Member using evolutive harmonic analysis and stratigraphic modeling. J. Sediment. Res. 71, 628–644.

Mundil, R., Brack, P., Meier, M., Reibner, H., Oberli, F., 1996. High resolution U-Pb dating of the Middle Triassic volcaniclastics: Time scale calibration and verification of tuning parameters for carbonate sedimentation. Earth Planet. Sci. Lett. 141, 137–151.

Mundil, R., Metcalfe, I., Ludwig, K.R., Renne, P.R., Oberli, F., Nicoll, R.S., 2001. Timing of the permian-triassic biotic crisis: implications from new zircon U/Pb age data (and their limitations). Earth Planet. Sci. Lett. 187, 131–145.

Olsen, P.E., 1986. A 40-million-year lake record of Early Mesozoic orbital climatic forcing. Science 234, 842–848.

Palfy, J., Parrish, R.R., Voros, A., 2002. Integrated U-Pb geochronology and ammonoid biochronology from the Anisian/Ladinian GSSP candidate section at Felsoors. STS/IGCP 467 Field Meeting, Abstract Volume, Vesprem, pp. 28.

Palike, H., Shackleton, N.J., Roehl, U., 2001. Astronomical forcing in late Eocene marine sediments. Earth Planet. Sci. Lett. 193, 589–602.

Park, J., Herbert, T.D., 1987. Hunting for paleoclimatic periodicities in a geologic time series with an uncertain time scale. J. Geophys. Res. 92, 14027–14049.

Parrish, J.T., 1993. Climate of the supercontinent Pangea. J. Geol. 101, 215–233.

Preto, N., Hinnov, L.A., Hardie, L.A., DeZanche, V., 2001. Middle Triassic orbital signature recorded in the shallow-marine Latemar carbonate buildup (Dolomites, Italy). Geology 29, 1123–1126.

Read, J.F., 1995. Overview of carbonate platform stratigraphy and reservoirs in green-house and ice-house worlds. In: Read, J.F., Kerans, C., Webber, L.J. (Eds.), Milankovitchian Sea Level Changes, Cycles and Reservoirs in Greenhouse and Ice-house Worlds. SEPM Short Course Notes 35.

Ripepe, M., Fischer, A.G., 1991. Stratigraphic rhythms synthesized from orbital variations. In: Franseen, K., Watney, W.L., Kendall, C.G.St.C., Ross, W. (Eds.), Sedimentary Modeling: Computer Simulations and Methods for Improved Parameter Definition. Kansas Geol. Surv. Bull. 233, 335–344.

Sadler, P.M., 1981. Sediment accumulation rate and the completeness of stratigraphic sections. J. Geol. 89, 569–584.

Sadler, P.M., 1994. The expected duration of upward-shallowing peritidal carbonate cycles and their terminal hiatuses. Geol. Soc. Am. Bull. 106, 791–802.

Sadler, P.M., 1999. The influence of hiatuses on sediment accumulation rates. In: Bruns, P., Hass, H.C. (Eds.), On the Determination of Sediment Accumulation Rates. GeoResearch Forum vol. 5, pp. 15–40.

Schubert, J.K., Bottjer, D.J., 1992. Early Triassic stromatolites as post-mass extinction disaster forms. Geology 20, 883–886.

Schubert, J.K., Bottjer, D.J., 1995. Aftermath of the Permian-Triassic mass extinction event: Paleoecology of Lower Triassic carbonates in the western USA. Paleogeogr. Paleoclimatol. Paleoecol. 116, 1–39.

Scotese, C.R., 1994. Early Triassic paleogeographic map. In: Klein, G.D. (Ed.), Pangea: Paleoclimate, Tectonics, and Sedimentation during Accretion, Zenith and Breakup of a Supercontinent. Geol. Soc. Am. Spec. Paper 288, Boulder, CO, p. 7.

Scotese, C.R., 2000. Gondwanan paleogeography and paleoclimatology. J. Afr. Earth Sci. 28, 99–114.

Sengör, A.M.C., 1987. Tectonics of the Tethysides-Orogenic collage development in a collisional setting. Annu. Rev. Earth Planet. Sci. 15, 213–244.

Stanley, G.D., Jr., 1988. The history of early Mesozoic reef communities: A three step process. Palaios 3, 170–183.

Sun, S., Li, J., Chen, H., Peng, H., Kenneth, J.H., Shelton, J.W., 1989. Mesozoic and Cenozoic sedimentary history of South China. Am. Assoc. Pet. Geol. Bull. 73, 1247–1269.

Thomson, D.J., 1982. Spectrum estimation and harmonic analysis. Proc. IEEE 70, 1055–1096.

Twitchett, R.J., 1999. Paleoenvironments and faunal recovery after the end-Permian mass extinction. Paleogeogr. Paleoclimatol. Paleoecol. 154, 27–37.

Twitchett, R.J., Wignall, P.B., 1996. Trace fossils and the aftermath of the Permo-Triassic mass extinction: evidence from northern Italy. Paleogeogr. Paleoclimatol. Paleoecol. 124, 137–151.

Van der Voo, R., 1993. Paleomagnetism of the Atlantic, Tethys and Iapetus Oceans. Cambridge University Press, Cambridge, 411 pp.

Wignall, P.B., Hallam, A., 1992. Anoxia as a cause for the Permian/Triassic mass extinction: Facies evidence from northern Italy and the western United States. Paleogeogr. Paleoclimatol. Paleoecol. 93, 21–46.

Wignall, P.B., Hallam, A., 1996. Facies change and the end-Permian extinction in S.E. Sichuan, China. Palaios 11, 587–596.

Wilkinson, B.H., Opdyke, B.N., Algeo, T.J., 1992. Time partitioning in cratonic carbonate rocks. Geology 19, 1093–1096.

Woods, A.D., Bottjer, D.J., Mutti, M., Morrison, J., 1999. Lower Triassic large sea-floor carbonate cements: Their origin and a mechanism for the prolonged biotic recovery from the end-Permian mass extinction. Geology 27, 645–648.

Woronow, A., 1992. A test of the γ method for evaluating the periodicity of cyclical sediments. Earth Planet. Sci. Lett. 113, 443–447.

Xü, X., Xü, Q., Pan, G., Liu, Q., 1997. Paleogeography of the south China continent and its contrast with Pangea. In: Liu, B., Li, S. (Eds.), Basin Analysis, Global Sedimentary Geology and Sedimentology. Int. Geological Congress, vol. 30, pp. 332–349.

Yang, W., 1996. Cycle symmetry and its causes: Cisco Group (Virgilian and Wolfcampian), Texas. J. Sediment. Res. 66B, 1102–1121.

Yang, W., Kominz, M.A., 1999. Testing periodicity of depositional cyclicity: Cisco Group (Virgilian and Wolfcampian), Texas. J. Sediment. Res. 69B, 1209–1231.

Yang, W., Lehrmann, D.J., 2001. Fischer plots constructed using variable cycle durations and their alternative sequence stratigraphic interpretation. Abstracts with Programs, 2001 Geol. Soc. Am. Annual Meeting, Boston, vol. 33, No. 6, p. A80.

Yang, W., Harmsen, F., Kominz, M.A., 1995. Quantitative analysis of a peri-tidal carbonate sequence, the Middle and Upper Devonian Lost Burro Formation, Death Valley, California - A possible Milankovitch climatic record. J. Sediment. Res. 65B, 306–322.

Yang, W., Lehrmann, D., Hiatt, E., Wei, J., Yu, Y., Wignall, P., 2002. Productivity-controlled peritidal carbonate cycles in a super-green-house climate in the aftermath of the end-Permian extinction, the Lower Triassic (Olenekian) Great Bank of Guizhou, South China. 2002 Am. Assoc. Pet. Geol. Annual Meeting, Official Program, Houston, TX, p. A194.

Yu, Y., Lehrmann, D.J., Wei, J., 1998. Relationships of the Early Triassic high-frequency cyclic deposition types in DaGuizhouTan, Southern Guizhou, with the periods of change of the orbit of the Earth [in Chinese, English abstract]. Reg. Geol. China 17, 1–8.